Molecular Therapy
Nucleic Acids
Original Article

RP11-616M22.7 recapitulates imatinib resistance in gastrointestinal stromal tumor

Yebo Shao,[1,2,5] Shixian Lian,[3,5] Jiajia Zheng,[2,5] Hanxing Tong,[2] Jiongyuan Wang,[2] Jing Xu,[2] Wenshuai Liu,[3] Guoxiang Hu,[4] Yong Zhang,[2] and Junyi He[2]

[1]Department of General Surgery, Zhongshan Hospital, Fudan University (Xiamen Branch), Xiamen 361015, China; [2]Department of General Surgery, Zhongshan Hospital, Fudan University, Shanghai 200032, China; [3]Department of General Surgery, Public Health Clinical Center, Shanghai 201508, China; [4]Department of Radiology, Zhongshan Hospital, Fudan University, Shanghai 200032, China

Emerging evidence has shown that long non-coding RNAs (lncRNAs) play crucial roles in human cancers. However, systematic characterization of lncRNAs and their roles in gastrointestinal stromal tumor (GIST) therapy have been lacking. We performed high-throughput RNA sequencing (RNA-seq) of 20 GIST and paired adjacent normal samples. We characterized the transcriptional landscape and dysregulation of lncRNAs in GIST. We identified 866 upregulated and 1,268 downregulated lncRNAs in GIST samples, the majority of which were GIST-specific over other cancer types. Most hallmarks were found to be dysregulated in GIST samples, and lncRNAs were highly associated with cancer-related hallmarks. RP11-616M22.7 was identified to increase in imatinib-resistant samples compared to those in non-resistant samples. Further analysis revealed that RP11-616M22.7 was closely associated with the Hippo signaling pathway. By treating GIST cells with different doses of imatinib, we verified that RP11-616M22.7 knockdown promotes the sensitivity of tumor cells, whereas RP11-616M22.7 overexpression induces resistance to imatinib. We further confirmed reducing of resistance to imatinib by knocking down RP11-616M22.7 *in vivo*. Additionally, RP11-616M22.7 was observed to interact with RASSF1 protein. Our study revealed that deficiency of RP11-616M22.7 was able to reduce resistance of the GIST cell response to imatinib treatment both *in vitro* and *in vivo*.

INTRODUCTION

Gastrointestinal stromal tumor (GIST) is the most common mesenchymal neoplasm of the gastrointestinal tact, comprising approximately 20% of all soft tissue sarcomas.[1] GIST primarily arises in the stomach or small intestine of patients, with median ages ranging from 60 to 65, which often causes bleeding, anemia, and pain. Approximately 60% of GIST patients with localized tumors are cured with surgery, which aims to completely excise macroscopic and microscopic GIST.[2] Tyrosine kinase inhibitors (TKIs) have shown promising therapeutic effects by substantially improving survival time for both patients with localized and advanced GIST. Three TKIs (e.g., imatinib, sunitinib, and regorafenib) have been approved for the management of advanced diseases, wherein imatinib is usually used in the standard first-line treatment.[1] In particular, adjuvant imatinib therapy benefits GIST patients with high-risk recurrence, while neoadjuvant imatinib therapy should be considered for GIST patients requiring extensive surgery. Although imatinib benefits most patients with advanced GIST, it has no or limited efficiency for some portions of GIST patients. Therefore, it is pressing to identify targets to promote imatinib treatment in imatinib-refractory GIST patients.

Long non-coding RNAs (lncRNAs), which are transcripts longer than 200 nt with no or limited protein-coding capability, have been shown to take part in a wide range of biological processes, exerting their functions by serving as scaffolds or guides regulating protein-protein or protein-DNA interaction, decoys binding proteins, and microRNA sponges.[3–5] Accumulating evidence has shown the crucial regulatory roles of lncRNAs in human cancers.[5–8] Moreover, recent studies suggested that lncRNAs could be targets for anti-cancer treatment or be able to mediate the sensitivity of tumor patients to existing anti-cancer agents.[6,9–11] Pichler et al.[9] discovered a novel primate-specific lncRNA, which was found to be upregulated in colorectal cancer samples, through analysis in 349 tumors from four cohorts. Further *in vivo* experiments showed that targeting FLANC by small interfering RNA (siRNA) carried by nanoparticles could reduce angiogenesis and metastases without inducing evident tissue toxicity or pro-inflammatory effects. In addition, Tan et al.[10] found that EGFR-AS1 knockdown was able to recapitulate the sensitivity, while overexpression could induce resistance, to TKIs both *in vitro* and *in vivo*.

In this study, we performed high-throughput RNA sequencing (RNA-seq) of 10 GIST samples with adjacent normal samples to characterize the transcriptional landscape and dysregulation of lncRNAs in GIST. We found that major hallmarks were dysregulated, wherein proliferation-related hallmarks were activated in GIST samples.

Received 9 November 2020; accepted 25 May 2021;
https://doi.org/10.1016/j.omtn.2021.05.017.

[5]These authors contributed equally

Correspondence: Junyi He, Department of General Surgery, Zhongshan Hospital, Fudan University, 180 Fenglin Road, Shanghai 200032, China.
E-mail: zhang.yong2@zs-hospital.sh.cn
Correspondence: Yong Zhang, Department of General Surgery, Zhongshan Hospital, Fudan University, 180 Fenglin Road, Shanghai 200032, China.
E-mail: he.junyi@zs-hospital.sh.cn

Additionally, lncRNAs were found to be highly linked to cancer-related hallmarks in GIST samples. We compared imatinib-resistant and non-resistant GIST samples to reveal imatinib sensitivity-related lncRNAs. We further validated that RP11-616M22.7 was able to promote the resistance of GIST cells to imatinib both *in vitro* and *in vivo*. Our study suggested RP11-616M22.7 as a potentially efficient biomarker for response of GIST patients to imatinib.

RESULTS

Transcriptional landscape and dysregulation of lncRNAs in GIST

In order to systematically interrogate the transcription of lncRNAs in GIST samples, we performed high-throughput RNA-seq for tumor and paired adjacent normal samples derived from 10 GIST patients. Specifically, five patients were resistant, while the other five patients responded well to imatinib treatment. The correlations among sequencing data were evaluated in four separate groups, including normal samples from imatinib-resistant patients, tumor samples from imatinib-resistant patients, normal samples from imatinib-sensitive patients, and tumor samples from imatinib-sensitive patients (Figure S1; Table S1). Samples in the same groups were highly correlated to each other with average correlations as 0.90, 0.92, 0.89, and 0.94, respectively. This observation indicates the high reliability of our sequencing data. The abundance of lncRNAs was further quantified in each sample (see Materials and methods). On average, we detected 6,240 lncRNAs, which constituted 39.55% of all annotated lncRNAs (Figure S2). Additionally, the majority of detected lncRNAs were expressed in low level with less than 10% of them expressed higher than 1 TPM. These observations were consistent with common transcription characteristics of lncRNAs in human tissues.[12,13] To examine the dysregulation of lncRNAs in GIST, we further performed differential analysis by comparing between tumor and paired normal samples (see Materials and methods). We identified 866 upregulated and 1,268 downregulated lncRNAs in GIST samples compared to adjacent normal samples (Figure 1A; Table S2). Most of the GIST differential lncRNAs were GIST-specific, wherein 51.87% (1,107 of 2,134) were specifically differential in GIST over other cancer types (Figure 1B). Meanwhile, a considerable portion (13.12%, 280 lncRNAs) showed extensive dysregulation across 19 cancer types. For example, lncRNA PGM5-AS1 was downregulated in 17 cancer types, including GIST (Figure 1C). In conclusion, our analysis characterized transcriptional landscape and dysregulation of lncRNAs in GIST, revealing GIST-specific differential lncRNAs.

GIST differential lncRNAs are closely associated with cancer-related hallmarks

We further aimed to investigate biological processes in which GIST differential lncRNAs may participate. Hallmark scores were first evaluated in each sample to examine the dysregulation of key biological processes in GIST (see Materials and methods). Compared to adjacent normal samples, 82% of hallmarks (41 of 50 hallmarks) were found to show aberrant activities in GIST samples (Figure 2A; Table S3). Proliferation hallmarks showed elevated activity in GIST, such as "G2M checkpoint," which is significantly activated in tumor samples (false discovery rate [FDR] = 0.00015, Figure 2B). This reflects the intensive proliferative activities in GIST cells. Moreover, most cancer signaling hallmarks exhibited decreased activities. For example, the overall activity of transforming growth factor β (TGF-β) signaling is significantly suppressed in GIST samples (FDR = 4.16E−05, Figure 2C). The TGF-β signaling pathway has been shown to inhibit tumorigenesis by inducing growth arrest and apoptosis, especially in the early stage tumor cells.[14] Our analysis suggested that inhibition of TGF-β signaling might be important for the initiation of GIST. The associations between hallmark biological processes and GIST differential lncRNAs were further assessed to explore the possible functions of GIST differential lncRNAs. We identified 47,907 statistically significant lncRNA-hallmark associations across GIST samples, wherein 69.67% (33,379 of 47,907) were positive associations (Figure S3; Table S4). Moreover, lncRNAs showed close links with many pivotal cancer-related hallmark processes in GIST, such as "KRAS signaling," "fatty acid metabolism," and "hypoxia" (Figure 2D). These results revealed that GIST differential lncRNAs were highly associated with key cancer-related hallmarks.

lncRNAs show distinct changes between imatinib-resistant and -sensitive GIST patients

As lncRNAs are associated with many cancer-related biological processes in GIST, they may be involved in regulating the treatment response to imatinib. To further investigate possible roles of lncRNAs in mediating the treatment response of GIST patients to imatinib, we performed differential analysis separately in imatinib-resistant and non-resistant patients. Both imatinib-resistant and non-resistant patients showed a larger number of downregulated lncRNAs than upregulated lncRNAs (Figures 3A and 3B). In particular, 810 and 465 lncRNAs were downregulated and upregulated in imatinib-resistant GIST samples, respectively (Figure 3C). Meanwhile, 1,306 downregulated and 285 upregulated lncRNAs were detected in imatinib-sensitive GIST samples in comparison with corresponding adjacent normal samples. By overlapping the sets of differential lncRNAs between imatinib-resistant and non-resistant GIST patients, we found 685 shared differential lncRNAs (Figure 3D). In addition, 590 lncRNAs were found to be specifically differential in imatinib-resistant GIST samples, whereas imatinib-sensitive GIST samples showed 509 exclusively differential lncRNAs. These discrepancies suggested that lncRNAs might modulate the treatment response of GIST patients to imatinib. To explore key lncRNAs that were involved in modulating imatinib resistance, we compared imatinib-resistant and non-resistant GIST samples directly. Consequently, we found 5 upregulated and 21 downregulated lncRNAs in imatinib-resistant GIST samples compared with imatinib-sensitive GIST samples (Figure 3E). For example, RP11-616M22.7 showed significantly higher expression in imatinib-resistant tumor samples in comparison with non-resistant tumor samples (FDR = 0.011, Figure 3F). Moreover, RP11-616M22.7 was remarkably upregulated in both imatinib-resistant (FDR = 0.00085) and non-resistant (FDR = 0.0040) GIST samples, suggesting that RP11-616M22.7 plays crucial roles in GIST. Collectively, our findings suggested that lncRNAs may mediate the resistance of GIST patients to imatinib.

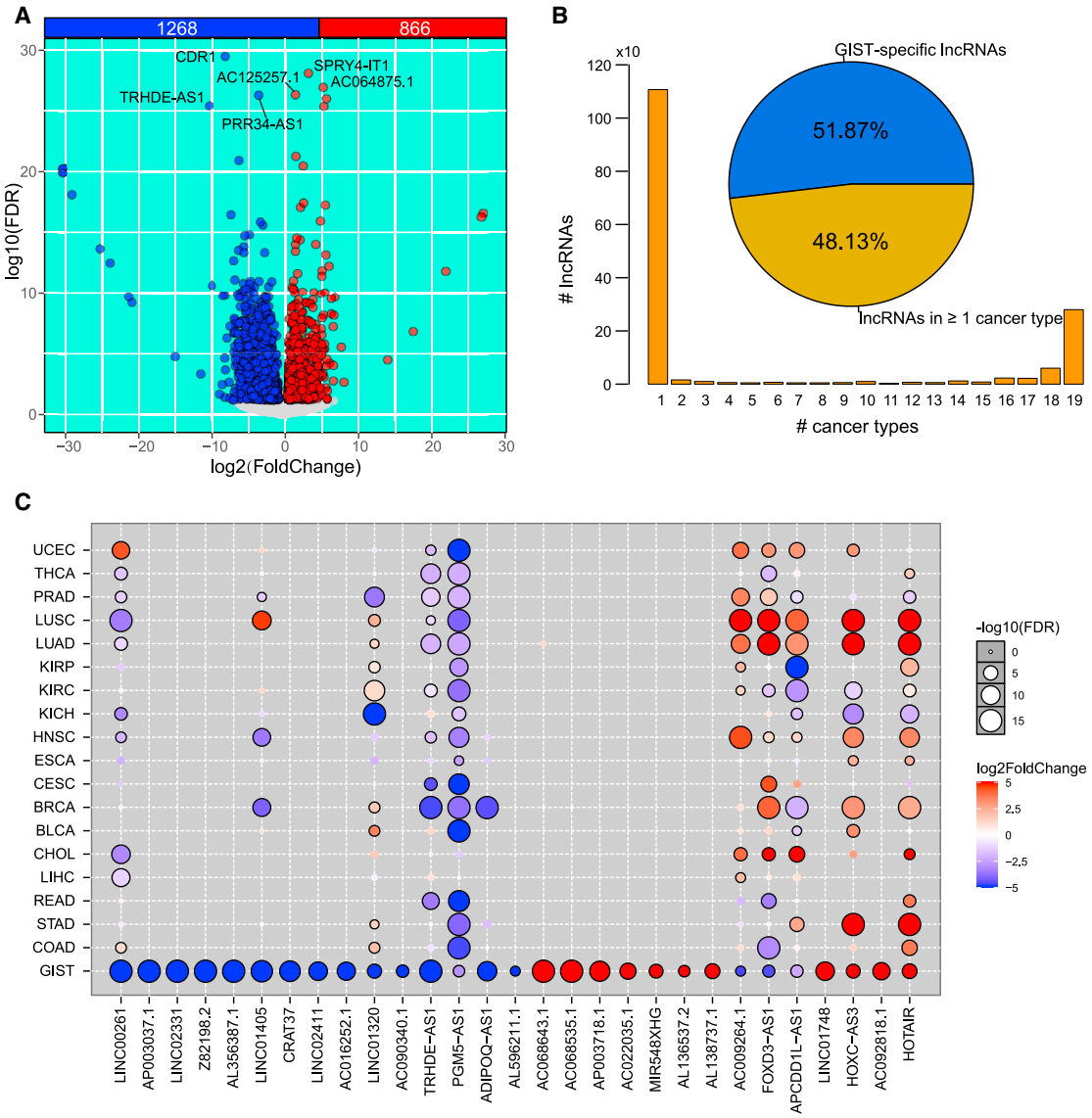

Figure 1. Expression dysregulation of GIST lncRNAs

(A) Volcano plot shows the differential lncRNAs in GIST samples compared to adjacent normal samples. Red dots indicate upregulated lncRNAs, and blue dots represent downregulated lncRNAs. (B) Distribution of cancer types that show differential expression of GIST-specific lncRNAs. (C) Expression difference of top GIST differential lncRNAs across 19 cancer types.

Characterization of lncRNA RP11-616M22.7 in GIST

Since RP11-616M22.7 showed hints in modulating imatinib resistance, we next systematically examined the characteristics of RP11-616M22.7 in GIST. RP11-616M22.7 locates in chromosome 10 and is marked with H3K27ac and DNase across multiple tumor cell lines, which indicates pervasive transcription of RP11-616M22.7 in tumor cells (Figure 4A). We then obtained the sequence of RP11-616M22.7 from the National Center for Biotechnology Information (NCBI) database (https://www.ncbi.nlm.nih.gov). The full length of RP11-616M22.7 was then determined by utilizing the 5′ and 3′ rapid amplification of complementary DNA ends (RACE) assays, which is 331 bp (Figure 4B). Through subcellular fractionation in GIST-882 cells, we found that RP11-616M22.7 was expressed more in nucleus than in cytoplasm (Figure 4C). The sequence of RP11-616M22.7 was predicted to be non-coding by multiple features (Figure S4). Furthermore, northern blotting analysis revealed distinct abundance of RP11-616M22.7 in cells treated with different doses of imatinib (Figure 4D). This observation showed the possible association between imatinib and RP11-616M22.7 expression in GIST cells. To explore the possible biological processes that RP11-616M22.7 may mediate, we performed gene set enrichment analysis (GSEA, see Materials and methods) in RP11-616M22.7 knockdown cells. RP11-616M22.7 was found to

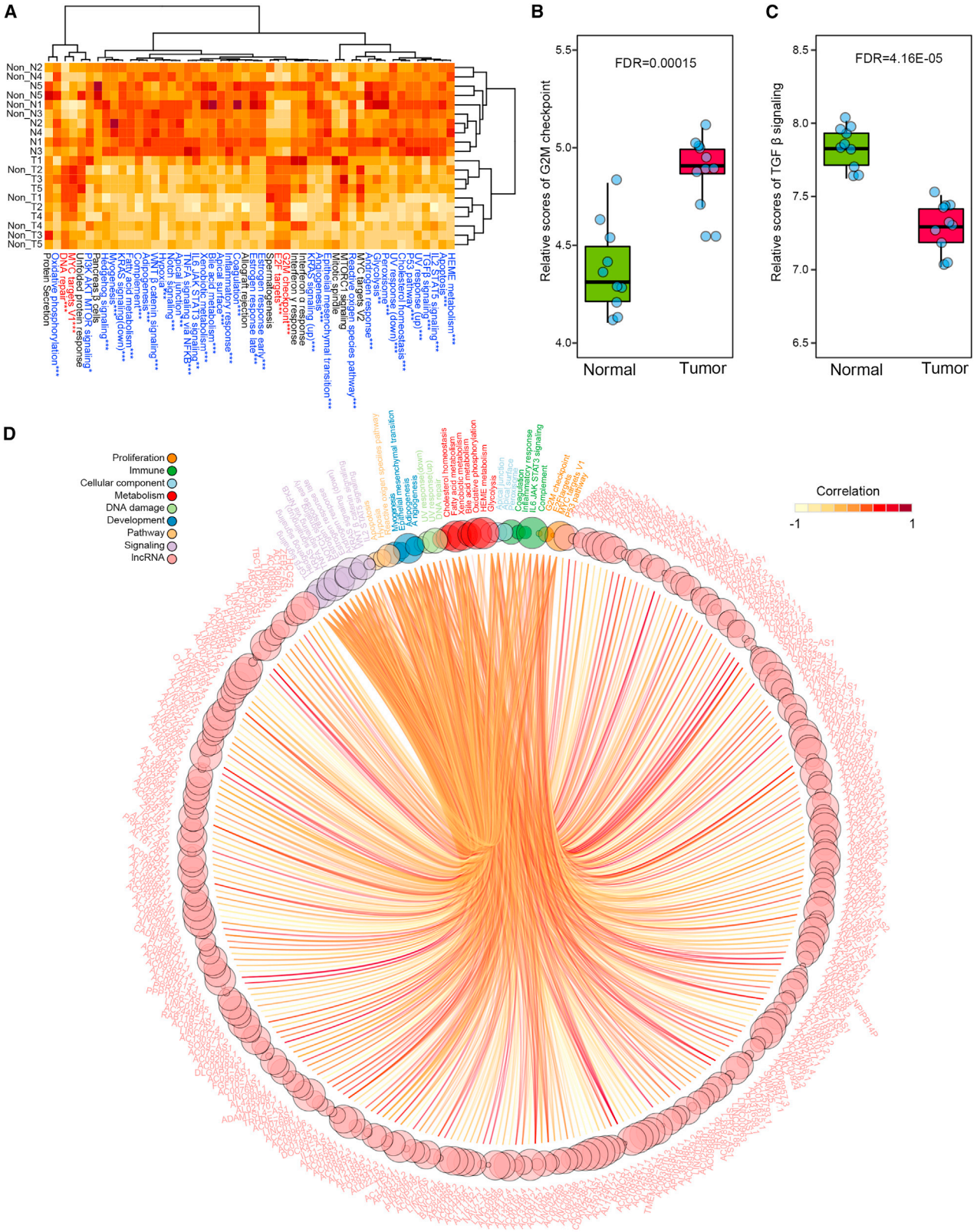

(legend on next page)

significantly interfere with multiple key cancer-related biological processes, such as "Hippo response," "allograft rejection," "myogenesis," "complement," "interleukin (IL)-6 JAK STAT3 signaling," "KRAS signaling," "angiogenesis," "IL-2 STAT5 signaling," and "UV response" (Figure 4E). In particular, genes in Hippo signaling were enriched in the bottom after RP11-616M22.7 knockdown (Figure 4F). To examine the importance of TGF-β and Hippo signaling for GIST cell growth, we performed cell proliferation experiments upon knockdown and overexpression of key genes (TGFRB1, SMAD2, WARTS, and YK1l). For all key genes, significant cell growth suppression was observed after knockdown, while overexpression of RP11-22.7M22.7 notably promoted GIST cell growth (Figure S5B). Our observations showed that RP11-616M22.7 is a non-coding RNA with no protein coding capability and may be associated with the treatment response of GIST patients to imatinib.

RP11-616M22.7 promotes resistance of GIST cells to imatinib

To further validate the function of RP11-616M22.7 in mediating treatment response of GIST patients to imatinib, we examined RP11-616M22.7 expression in cells treated with different doses of imatinib. The expression level of RP11-616M22.7 was found to increase with the increment of imatinib doses (Figure 5A). We next examined RP11-616M22.7 expression in another cohort of GIST patients, including imatinib-resistant and non-resistant patients. RP11-616M22.7 was found to significantly differentially express in both imatinib-resistant ($p = 0.0005$) and non-resistant tumor samples ($p = 0.0025$) compared to corresponding adjacent normal samples (Figure 5B). Moreover, imatinib-resistant GIST samples exhibited a remarkably higher expression level than did imatinib non-resistant tumor samples ($p = 0.0114$). Furthermore, a higher genomic copy number of RP11-616M22.7 was found in imatinib-resistant patients in comparison with non-resistant patients ($p = 0.0215$, Figure 5C), suggesting a possible genomic mechanism of RP11-616M22.7 high expression. These results were consistent with those in our RNA-seq data. Moreover, RP11-616M22.7 showed significantly higher expression in the VIM(+) group than in the VIM(−) group ($p < 0.0001$, Figure 5D). We further knocked down RP11-616M22.7 in GIST-882 cells treated with different doses of imatinib. In contrast to the control, the growth ability of GIST-882 cells receded significantly after RP11-616M22.7 knockdown, especially in high-dose imatinib treatment groups (Figure 5E). Meanwhile, GIST-T1 cells with overexpressed RP11-616M22.7 showed high growth ability after imatinib treatment (Figure 5F). Furthermore, the migratory ability of GIST-882 cells decreased with high-dose imatinib treatment after RP11-616M22.7 knockdown (Figure 5G), whereas RP11-616M22.7 overexpression enhanced migration of GIST-T1 cells with high-dose imatinib treatment (Figure 5H). Our results showed that high expression of RP11-616M22.7 was highly associated with imatinib resistance in GIST cells.

In vivo validation of RP11-616M22.7 promoting GIST resistance to imatinib

We further validated the impact of RP11-616M22.7 on imatinib resistance in GIST mice models (see Materials and methods). The mice injected with GIST-T1 cells were divided into four groups (n = 5 in each group), including siRNA negative control (siNC), siRP11-616M22.7, siNC+imatinib treatment, and siRP11-616M22.7+imatinib treatment (Figure 6A). In the siNC+imatinib and siRP11-616M22.7+imatinib treatment groups, imatinib treatment started in the seventh day. The mice in the siRP11-616M22.7-+imatinib treatment group showed the longest overall survival time compared with those in other groups. Meanwhile, the tumor weights derived from siRP11-616M22.7+imatinib treatment were the lowest. In addition, we found that mice injected with siRP11-61622.7 followed by imatinib treatment exhibited remarkably smaller tumor than did those injected with siNC followed by imatinib treatment (Figure 6B). These results demonstrated that RP11-616M22.7 knockdown promotes imatinib treatment efficiency on GIST cells, which suggested a promising therapeutic strategy for GIST patients. To better understand how RP11-616M22.7 performs its impact on GIST resistance to imatinib, we conducted RNA pull-down assays to identify possible proteins that interact with RP11-616M22.7. The mass spectrometry analysis following RP11-616M22.7 pull-down experiments revealed specific protein bands of RASSF1 for only the sense but not anti-sense strand of RP11-616M22.7 (Figure 6C). Further real-time PCR analysis in both GIST-T1 and GIST-882 cell lines confirmed that RASSF1 was specifically associated with the sense but not anti-sense strand of RP11-616M22.7 (Figure 6D). RP11-616M22.7-RASSF1 interaction was further verified by an RNA immunoprecipitation (RIP) assay. In particular, RP11-616M22.7 was significantly enriched in RASSF1 antibody but not in the immunoglobulin G (IgG) control (Figure 6E). We further performed cell proliferation and migration experiments upon RASSF1 gene knockdown. GIST-T1 cells with RP11-616M22.7 and siRASSF1A showed significantly suppressed ability of proliferation and migration. These observations demonstrated that RP11-616M22.7 exerts its biological function through RASSF1 protein (Figure 6F). We examined the relative expression of RASSF1 downstream genes, including MST1, MST2, LATS1, LATS2, YAP, and TAZ, upon RP11-616M22.7+siNC and RP11-616M22.7+siRASSF1A. Through interacting with RASSF1A, RP11-616M22.7 could upregulate the expression levels of MST1, MST2, LATS1, and LATS2, whereas it downregulated YAP and TAZ (Figure S6B). Furthermore, we performed cell proliferation experiments of GIST-T1 treated with mock, DMSO, 20 μM imatinib, and 40 μM imatinib. When compared to the control, knockdown of RASSF1 significantly reduced imatinib resistance, indicating that RP11-616M22.7 mediates imatinib resistance through binding of RASSF1 protein (Figure S6C). Additionally, we

Figure 2. Dysregulation of hallmark functions in GIST samples

(A) Heatmap shows the relative scores of 50 hallmarks in GIST and adjacent normal samples. (B) Comparison of relative scores of "G2M checkpoint" between GIST and adjacent normal samples. (C) Comparison of relative scores of "TGF β signaling" between GIST and adjacent normal samples. (D) The associations between lncRNAs and hallmarks. Only lncRNAs that were significantly ($|r_s| \geq 0.8$) associated with more than 5 hallmarks were shown. *$p < 0.05$; **$p < 0.01$; ***$p < 0.001$.

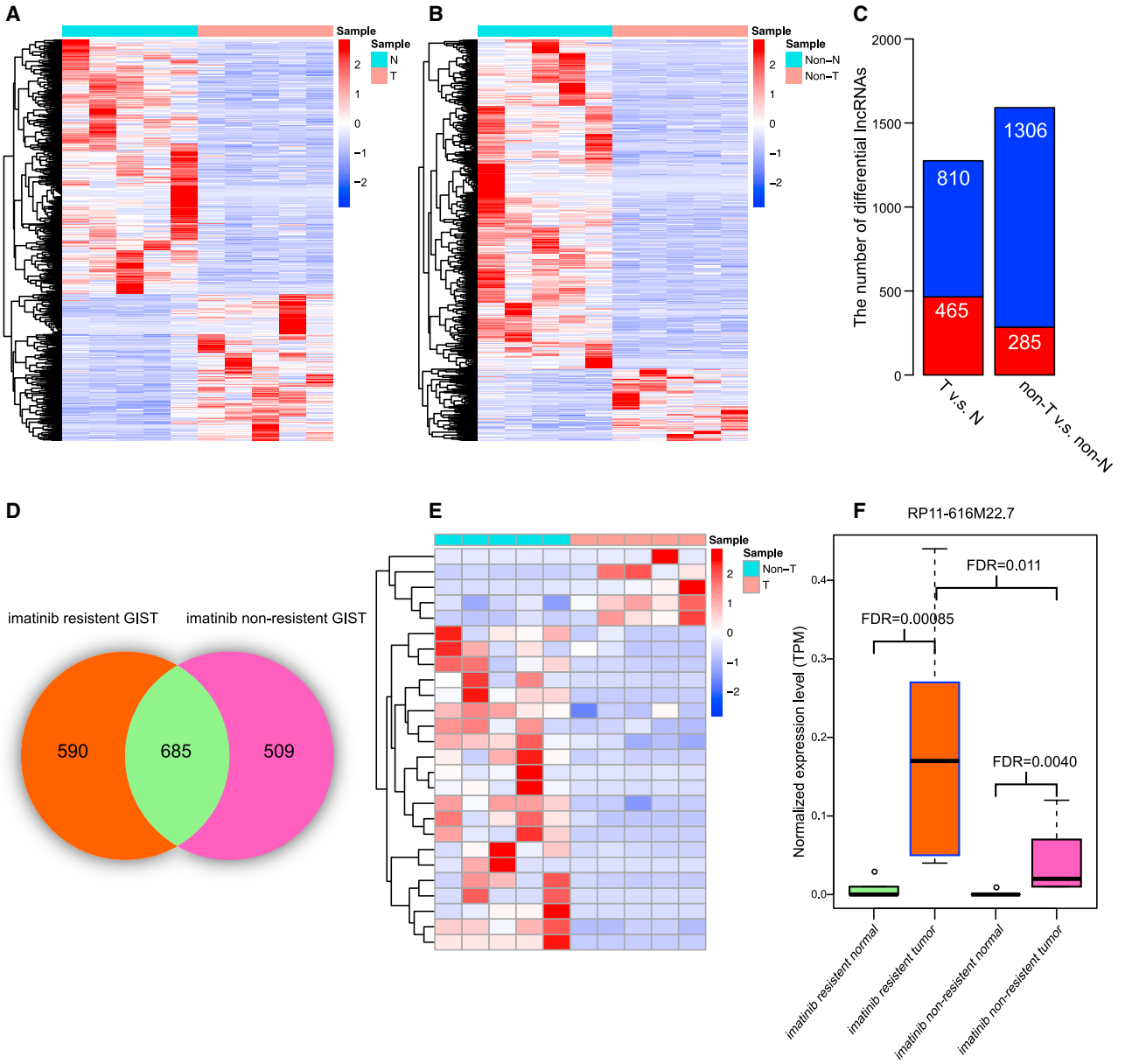

Figure 3. Differential lncRNAs in imatinib-sensitive and resistant GIST samples

(A) Heatmap displays differential lncRNAs in imatinib-resistant GIST samples compared to corresponding adjacent normal samples. (B) Heatmap shows differential lncRNAs in imatinib-sensitive GIST samples compared to adjacent normal samples. (C) Number of upregulated and downregulated lncRNAs in imatinib-resistant and -sensitive GIST samples. (D) Overlapping of differential lncRNAs between imatinib-resistant and -sensitive GIST samples. (E) Heatmap shows the expression variations of differential lncRNAs in imatinib-resistant GIST samples compared to imatinib-sensitive GIST samples. (F) Comparisons of RP11-616M22.7 relative expression in imatinib-resistant and -sensitive GIST samples with corresponding adjacent normal samples.

performed cell proliferation and migration experiments upon knockdown and overexpression of RP11-616M22.7 in both GIST-T1 and GIST-882. In both cell lines, RP11-616M22.7 overexpression promoted cell proliferation and migration, while knockdown suppressed cell growth and migration (Figure S6D). These results suggested that RP11-616M22.7 may promote GIST resistance to imatinib by interacting with RASSF1 protein.

DISCUSSION

By analyzing in-depth high-throughput RNA-seq data, our study presented the first comprehensive characterization of the lncRNA landscape in GIST and its association with imatinib resistance. This study will promote understanding of the noncoding transcriptome of GIST. Our analysis found that GIST samples expressed ~40% of all annotated lncRNAs in humans. We identified 866 upregulated and 1,268

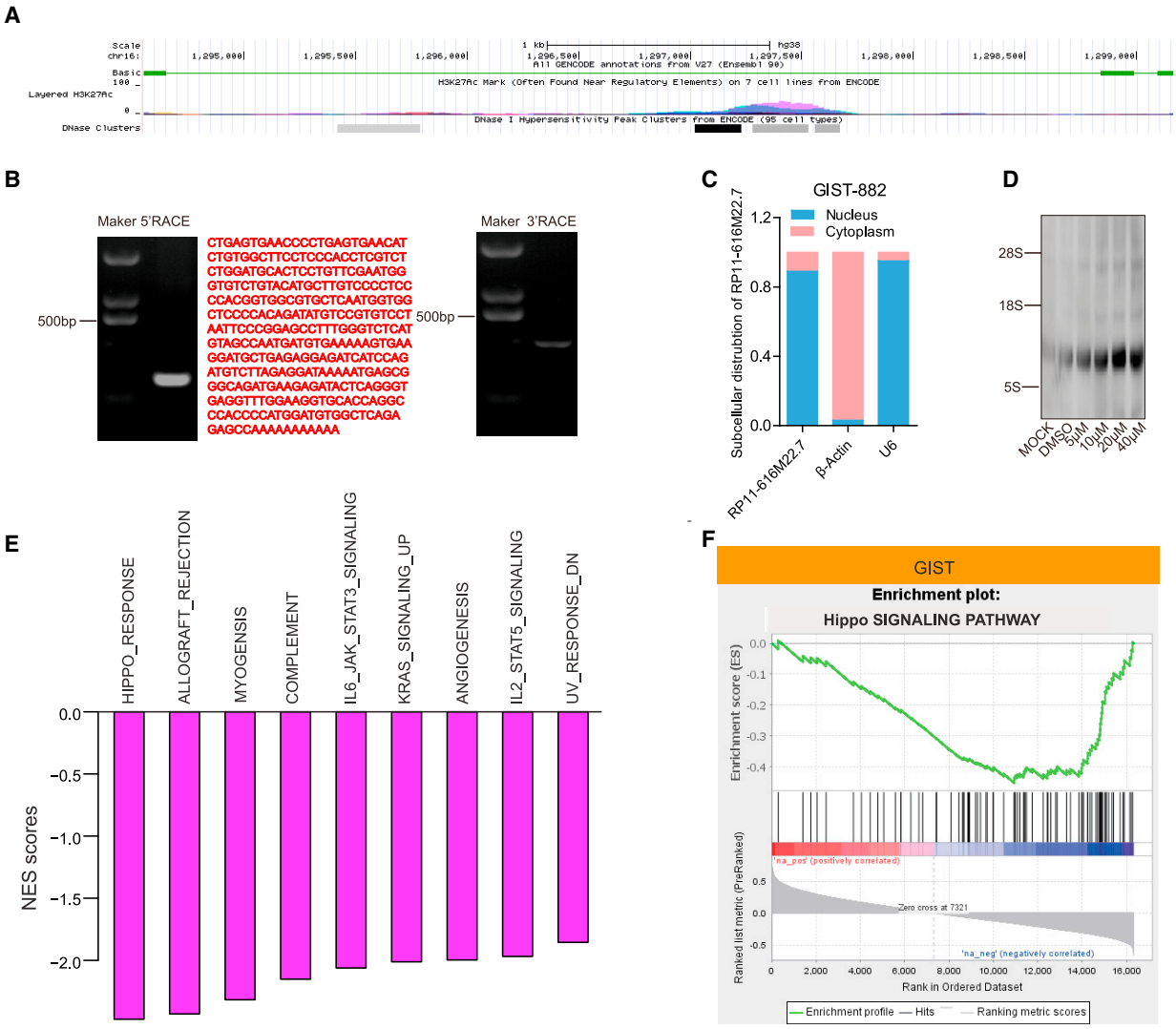

Figure 4. Genomic features of RP11-616M22.7

(A) Genomic position and chromatin status of RP11-616M22.7. (B) Determination of the full-length RP11-616M22.7 in GIST-882 cells by 5′ and 3′ RACE. (C) Distribution of RP11-616M22.7 in cytoplasm and nucleus of GIST-882 cells. β-Actin serves as a cytoplasmic marker and U6 serves as a nuclear marker. (D) Northern blot analysis of RP11-616M22.7 in GIST-882 cells treated with different doses of imatinib. (E) Enriched hallmarks of differentially expressed genes after RP11-616M22.7 knockdown. (F) GSEA results of the Hippo signaling pathway.

downregulated lncRNAs in GIST samples, most of which are GIST-specific. We compared the activities of 50 key biological hallmarks between GIST and normal samples. We found that proliferation hallmarks showed elevated activity in GIST, such as "G2M checkpoint." Most cancer signaling hallmarks exhibited decreased activities, such as "TGF-β signaling." GIST differential lncRNAs were found to be highly associated with key cancer-related hallmarks, wherein we identified 47,907 statistically significant lncRNA-hallmark associations across GIST samples. Furthermore, by comparing imatinib-resistant and non-resistant GIST samples, we identified lncRNAs that possibly mediate the sensitivity of GIST patients to imatinib. In particular, we identified 5 upregulated and 21 downregulated lncRNAs in imatinib-resistant GIST samples compared with imatinib-sensitive GIST samples, among which RP11-616M22.7 showed significantly higher expression in imatinib-resistant tumor samples. We characterized the genomic features and further verified the ability of RP11-616M22.7 to recapitulate resistance to imatinib both *in vitro* and *in vivo*. Specifically, the growth ability of GIST-882 cells receded significantly after RP11-616M22.7 knockdown, especially in high-dose imatinib treatment groups. Meanwhile, GIST-T1 cells with overexpressed RP11-616M22.7 showed high growth ability after imatinib treatment. In GIST mouse models, the siRP11-616M22.7-+imatinib treatment group showed the longest overall survival time and smallest tumor sizes compared with other groups. We also found

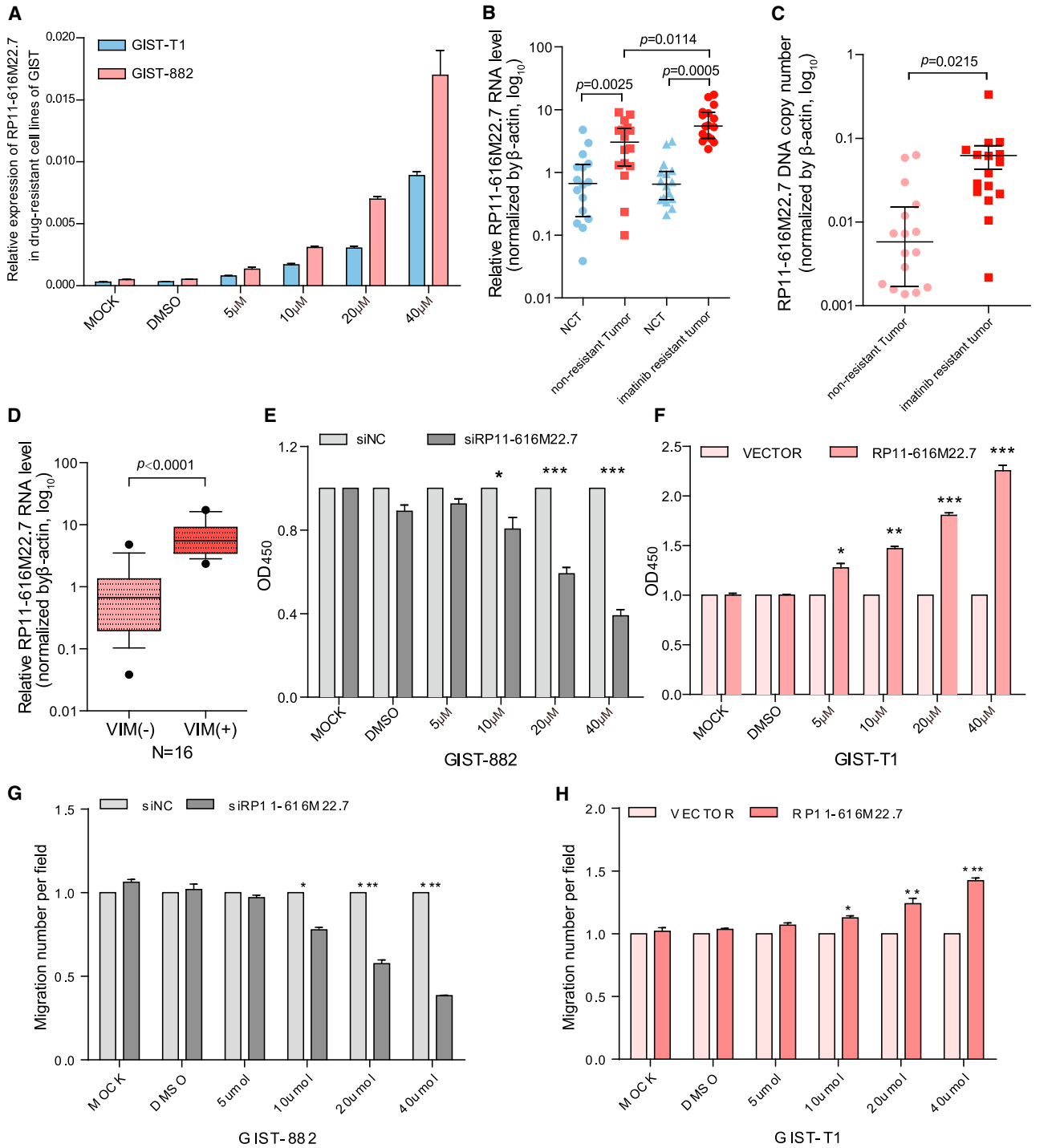

Figure 5. *In vitro* validation of RP11-616M22.7 impact on response of GIST cells to imatinib

(A) Relative expression of RP11-616M22.7 in GIST-T1 and GIST-882 cells treated with different doses of imatinib. (B) Comparisons of RP11-616M22.7 relative expression levels in imatinib-resistant and non-resistant GIST samples compared to corresponding adjacent normal samples. (C) Comparison of RP11-616M22.7 copy numbers between samples derived from imatinib-resistant and non-resistant GIST patients. (D) Comparison of RP11-616M22.7 relative expression level between VIM(−) and VIM(+) groups. (E) Comparison of cell proliferation between siNC and siRP11-616M22.7-transfected GIST-882 cells treated with different doses of imatinib. (F) Comparison of cell proliferation between vector and RP11-616M22.7-transfected GIST-T1 cells treated with different doses of imatinib. (G) Comparison of

(legend continued on next page)

that RP11-616M22.7 may promote GIST resistance to imatinib by interacting with RASSF1 protein.

We found that most GIST differential lncRNAs were GIST-specific. This observation was consistent with the tissue-specific feature of lncRNAs.[12,13,15] By comprehensively analyzing lncRNAs in 5,037 human tumor samples across 13 cancer types, Yan et al.[13] revealed that the expression and dysregulation of lncRNAs are more cancer type-specific than are protein-coding genes. Thus, our finding is compatible with basic biological features of lncRNA in human cancer. Furthermore, GIST-specific differential lncRNAs may be involved in biological functions that are exclusive in the development or therapy of GIST. Further investigation in these lncRNAs will facilitate carcinogenesis progress of GIST and accelerate the development of discovering novel efficient targets for GIST therapy.

Most of the cancer-related signaling hallmarks were found to be suppressed in GIST samples, such as "TGF-β signaling" and "phosphatidylinositol 3-kinase (PI3K) AKT MTOR signaling." Some pathways were demonstrated to be tumor suppressing pathways in many cancers, such as "P53 pathway."[16] The inactivation of these pathways was not surprising that suppressing these pathways leads to tumor initiation. In particular, the p53 pathway responds to a variety of intrinsic and extrinsic stress signals that affect such cellular homeostatic mechanisms as monitoring DNA replication, chromosome segregation, and cell division, which are frequently disrupted in tumor initiation.[17] Other signaling pathways, such as "TGF-β signaling," were reported to be suppressed in the early stage of cancer.[14] Activating these pathways may inhibit the progression of tumor, which suggested a potential therapeutic intervention at the beginning of tumor. Specifically, in early tumor cells, TGF-β acts as a potent growth inhibitor that halts cell cycle progression by increasing expression of the CDK inhibitors, such as p15 (INK4), p21 (CIP1), p27 (KIP1), and p57 (KIP2).[18] Tumor cells are able to escape the tumor-suppressive effects of TGF-β when the TGF-β signaling pathway is inactivated or subverted.

Our analysis demonstrated that RP11-616M22.7 could recapitulate imatinib resistance both *in vitro* and *in vivo*. We first compared the samples derived from imatinib-resistant and -sensitive patients, revealing a higher expression level of RP11-616M22.7 in imatinib-resistant samples. We treated GIST cells with different doses of imatinib. GIST cells with siRP11-616M22.7 were more sensitive to imatinib, especially higher doses. We further validated the promoting effects of siRP11-616M22.7 on imatinib sensitivity in GIST mouse models. Our results proposed a novel therapeutic strategy for GIST patients that the combination of imatinib and RP11-616M22.7 inhibitor is promisingly efficient for imatinib-resistant GIST patients. Further verification that includes more animal experiments and other pre-clinical trials is needed before human clinical trials and implementation. The improvement of RP11-616M22.7 inhibitor delivery, such as nanoparticles, will also expedite the application of this novel therapeutic strategy.

We further found that RP11-616M22.7 interacts with RASSF1 protein. RASSF1 is involved in regulation of the Hippo signaling pathway,[19] which is consistent with our function enrichment analysis. RP11-616M22.7-RASSF1 interaction was further verified by RNA pull-down and RIP experiments. In our RNA-seq data, RP11-616M22.7 showed no significant association with the RASSF1 gene across GIST samples (Figure S6A). The slightly negative correlation may indicate that RP11-616M22.7 might negligibly impact RASSF1 gene expression, but this observation needs further validation due to the small sample size in the present study. Our analysis demonstrated the interaction between RP11-616M22.7 and RASSF1. Further experiments and larger cohorts are needed to reveal how RP11-616M22.7 interacts with RASSF1 proteins and to determine the elaborate mechanism by which RP11-616M22.7 mediates the response of GIST cells to imatinib through RASSF1 proteins. KIT/platelet-derived growth factor receptor alpha (PDGFRA) are well-known drivers in GIST.[20] To investigate the relationship between RP11-616M22.7 and KIT/PDGFRA and the downstream intermediates PI3K/AKT/mTOR and RAF/mitogen-activated protein kinase (MAPK), we performed knockdown and overexpression of RP11-616M22.7 in GIST-882 and GIST-T1 cell lines. Then, the relative expression levels of KIT/PDGFRA/PI3K/AKT/mTOR/RAF/MAPK were quantified and compared with the control. We found that RP11-616M22.7 could significantly affect the expression of KIT and PI3K/AKT, but it had limited influence on the expression of PDGFRA, mTOR, and RAF/MAPK (Figures S7 and S8). Although KIT is a driver of GIST cells, our study demonstrated that RP11-616M22.7 could promote GIST resistance to imatinib through RASSF1.

MATERIALS AND METHODS

Cell lines and human clinical samples

The GIST cell lines GIST-T1 and GIST-882 were purchased from the American Type Culture Collection (ATCC, Manassas, VA, USA). GIST cell lines were then generated through 3 months of drug resistance, and we examined the imatinib resistance marker protein to determine whether the resistant cell lines were constructed successfully. All GIST clinical tissues in this study were obtained with clinical information (Table S1) from the surgical specimen archives of Fudan University Zhongshan Hospital, Shanghai, China. All human tissue acquisitions have written informed content from patients, and this study was approved by the Clinical Research Ethics Committee of Fudan University Zhongshan Hospital.

High-throughput RNA-seq

Total RNA samples (3 μg) were collected by using TRIzol reagent (Invitrogen, Waltham, MA, USA). The collected RNA samples were then

cell migration between siNC and siRP11-616M22.7-transfected GIST-882 cells treated with different doses of imatinib. (H) Comparison of cell migration between vector and RP11-616M22.7-transfected GIST-T1 cells treated with different doses of imatinib. Values are indicated as mean ± SEM in (A) and (E)–(H). *$p < 0.05$, **$p < 0.01$, ***$p < 0.001$.

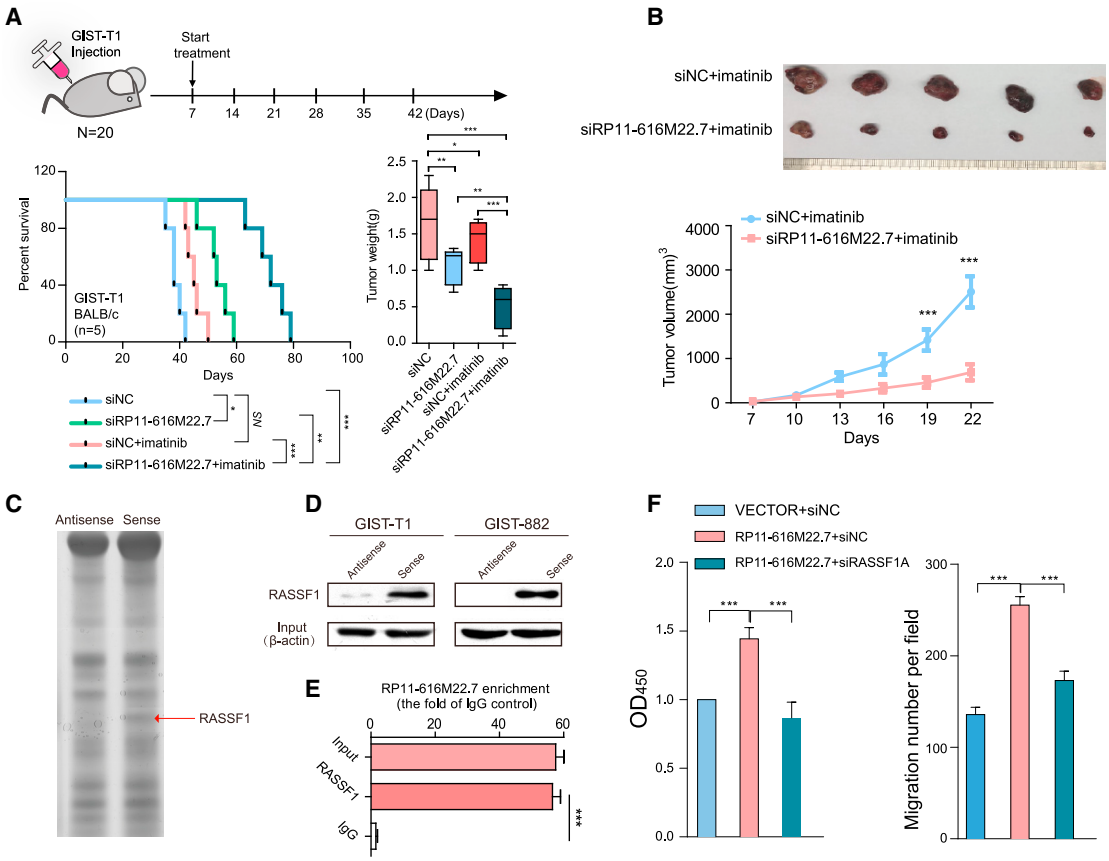

Figure 6. *In vivo* validation of RP11-616M22.7 and possible function mechanism

(A) Survival analysis of four different mouse groups injected with GIST-T1 cells transfected with siNC, siRP11-616M22.7, siNC+imatinib, and siRP11-616M2.7+imatinib. (B) Comparison of tumor growth between mice in siNC+imatinib and siRP11-616M22.7+imatinib groups. (C) RP11-616M22.7 pull-down assay analyzed by SDS-PAGE. (D) Western blot analysis of the RASSF1 protein retrieved from RP11-616M22.7 pull-down assay. (E) Quantitative real-time PCR results of RIP assay using an anti-RASSF1 antibody. (F) Comparisons of cell proliferation and migration abilities between GIST-T1 cells transfected with RP11-616M22.7+siRASSF1A and RP11-616M22.7+siNC. Values are indicated as mean ± SEM in (A), (B), and (E). *p < 0.05, **p < 0.01, ***p < 0.001.

treated with the RiboMinus eukaryote kit (QIAGEN, Valencia, CA, USA) to remove ribosome RNAs before constructing RNA-seq libraries. Strand-specific sequencing libraries were prepared by the NEBNext Ultra directional RNA library prep kit for Illumina (New England Biolabs, Beverly, MA, USA) per the manufacturer's instructions. All raw sequencing reads were deposited in the Gene Expression Omnibus (GEO) database under accession code GEO: GSE155800.

Processing RNA-seq data

The raw sequencing reads were first trimmed by the Trimmomatic (version 0.36) program[21] to remove adaptor sequences and low-quality bases with the following settings: ILLUMINACLIP:adaptor:2:30:10 LEADING:3 TRAILING:3 SLIDINGWINDOW:4:15 MINLEN:36. Trimmed sequencing reads were then subjected to STAR[22] software (version 2.7.3a) to align to the human reference genome (hg38) with default parameters. Then, RSEM (version 1.3.2) software[23] was used to quantify gene expression with gene annotation from GENCODE version 27.[24] Read count quantifications of genes generated from RSEM were used for differential expression analysis by the DESeq2 (version 1.0) package.[25] Genes with a FDR <0.05 and |fold change| >1.5 were regarded as statistically significant.

Pan-cancer expression analysis of GIST differential lncRNAs

We downloaded RNA-seq gene expression profiles of 18 cancer types with more than five paired tumor and adjacent normal samples from the Genomic Data Commons (GDC) data portal[26] (https://portal.gdc.cancer.gov/). The expression matrix of all lncRNAs in multiple cancer types was extracted by using a customized Python script. The raw read count profile of lncRNAs was then subject to DESeq2 to determine the expression changes in tumor samples. Cancer types with a |fold change| >1.5 and a FDR <0.05 were considered to express differential lncRNAs. lncRNAs that were identified to differentially express in only one cancer type were defined as cancer-specific differential lncRNAs.

Calculation of hallmark scores in GIST samples

The gene sets of 50 hallmarks were retrieved from the Molecular Signature Database (MSigDB),[27] which includes eight function categories, i.e., "Cellular component," "Immune," "Development," "Pathway," "Metabolic," "Signaling," "DNA damage," and "Proliferation." Then, the activity variations of each hallmark were assessed in each single GIST sample by using the gene set variation analysis (GSVA) method.[28] In particular, the hallmark scores were calculated based on the expression profiles of genes annotated in corresponding hallmarks. The Spearman rank correlations were used to determine the associations between differential lncRNAs and hallmarks. Associations with a $|r_s| > 0.5$ and a FDR <0.05 were considered statistically significant.

5′ and 3′ RACE assay

A RACE assay was adapted to determine the full length of RP11-616M22.7. Specifically, 5′ and 3′ RACE assays were performed to determine the transcriptional initiation and termination sites of RP11-616M22.7. The SMARTer RACE cDNA amplification kit (Clontech Laboratories, CA, USA) was used according to the manufacturer's instructions.

Subcellular fractionation

We used a nuclear/cytoplasmic isolation kit (Thermo Fisher Scientific, Carlsbad, CA, USA) to extract the cytoplasmic and nuclear fraction of GIST-882 cells per the manufacturer's instructions. In addition, β-actin was used as a cytoplasmic endogenous control and U6 RNA was used as a nuclear endogenous control.

Quantitative real-time PCR assay

Total RNAs were extracted from clinical tissues and cell lines by using TRIzol reagent (Invitrogen, Carlsbad, CA, USA). The reverse transcriptase kit (Takara Bio, Dalian, China) was used to reversely transcribe the extracted total RNA into cDNA in the LifePro thermal cycler (Hangzhou Bioer Technology, Hangzhou, China). Then, relative RNA levels were determined by quantitative real-time PCR on the 7900 real-time PCR system with a SDS v2.3 software sequence detection system (Applied Biosystems, Waltham, MA, USA) with the SYBR Green (Takara Bio, Kusatsu, Shiga, Japan) method. In particular, RNA levels were normalized by using β-actin as the internal control in each sample and calculated by utilizing the $2^{-\Delta\Delta Ct}$ relative quantification method as described in a previous study.[11]

GSEA

GSEA was performed to investigate the biological processes that RP11-616M22.7 may affect, for which we used GSEA software (https://www.gsea-msigdb.org/gsea/index.jsp).[29] In particular, the gene expression profiles of RP11-616M22.7 knockdown and control were subject to GSEA to test the enrichment of most changed genes among various biological processes. The gene sets of biological processes were downloaded from the MSigDB database.

Northern blot assays

To detect RP11-616M22.7 levels in tissues and cells, we used the nitrocellulose (NC) membrane with a positive charge to electrophorese and siphon the extracted total RNA samples. Then, UV cross-linking was conducted to fix RNAs on the NC membrane. Finally, a digoxin (DIG)-labeled RP11-616M22.7-specific oligonucleotide probe was used to detect the RP11-616M22.7 level in a DIG Northern Starter kit (Roche, Indianapolis, IN, USA). These assays were performed by using the Ambion NorthernMax-Gly kit (Ambion, Austin, TX, USA).

Western blot assays

Proteins were separated by SDS-PAGE then transferred to NC membranes (Bio-Rad, Hercules, CA, USA). Specifically, NC membranes were blocked with 5% nonfat milk and incubated with corresponding primary antibodies and horseradish peroxidase-conjugated secondary antibodies. The immunoreactivity was visualized by chemiluminescence and enhanced chemiluminescence (ECL) reagents (Pierce Biotechnology, Rockford, IL, USA). The Image-Pro Plus 6.0 (Media Cybernetics, Rockville, MD, USA) was used to determine the densitometry.

RNA interference and lentivirus construction

For RNA interference (RNAi), the siRNA oligonucleotides of RP11-616M22.7 in the present study were purchased from RiboBio (Guangzhou, China). Human RP11-616M22.7 was amplified from cDNA. RP11-616M22.7 RNAi experiments were conducted in the GIST-882 cell line. To generate overexpressed RP11-616M22.7, the RP11-616M22.7 sequence was cloned into the BamHI and EcoRI sites of pWPXL lentiviral vectors. Then, pWPXL and PWPXL-RP11-616M22.7 were transfected into the GIST-T1 cell line with packaging plasmid psPAX2 and the envelope plasmid pMD2 by using Lipofectamine 2000 (Invitrogen, Waltham, MA, USA) per the manufacturer's instructions. The virus particles were collected after 48 h of transfection. Then, GIST cells were transfected with recombinant lentivirus-transducing units by using 1 μg/mL Polybrene (Sigma-Aldrich, St. Louis, MO, USA). The relative expression levels of RP11-616M22.7 were evaluated upon overexpression and knockdown of RP11-616M22.7 in GIST-T1 and GIST-882 cell lines, respectively, which displayed high efficiency of overexpression and knockdown of RP11-616M22.7 (Figure S5A).

Cell proliferation assays

The cells were seeded in 96-well flat-bottomed plates, with each well containing 1,500 cells in 100 μL of cell suspension. After a certain time in culture, cell viability was measured using Cell Counting Kit-8 (CCK-8) assays (Dojindo, Kumamoto Prefecture, Japan). Each experiment with six replicates was repeated three times and measured continuously for 5 days.

Cell migration assays

Millicell chambers were used to perform cell migration assays in triplicates. In particular, cells (5×10^4) were added to the coated filters in serum-free medium. DMEM (10% fetal bovine serum [FBS]) was added to the lower chambers as a chemoattractant. Then, cells were incubated at 37°C with 5% CO_2 for 24 h. Cells migrating through the filters were fixed with methanol and stained with crystal violet. Five random fields were chosen to count cell numbers.

RNA pull-down assays and mass spectrometry analyses

First, RP11-616M22.7 and antisense RP11-616M22.7 were separately transcribed and labeled by a biotin RNA labeling mix (Roche, USA). Then, they were treated with RNase-free DNase I (Takara, Japan) and purified with the RNeasy mini kit (QIAGEN, USA). Second, RNA structure buffer (Beyotime Biotechnology, Shanghai, China) was used to treat biotinylated RNA (1 pmol) to obtain an appropriate secondary structure. Then, pre-treated biotinylated RNAs were incubated with 1 mg of protein extracts from GIST-882 cells at 4°C for 1 h. These RNAs were fixed with 40 μL of washed streptavidin beads (Invitrogen, USA) and incubated on a rotator overnight. Next, the beads were washed five times in 1× washing buffer (5 mM Tris-HCl, 1 M NaCl, 0.5 mM EDTA, and 0.005% Tween 20). Finally, the proteins were precipitated and diluted in 60 μL of protein lysis buffer, separated by gel electrophoresis, and visualized by silver staining. Specific bands were excised for proteomics screening by mass spectrometry analysis (Shanghai Applied Protein Technology, Shanghai, China). Protein identification was retrieved in the human RefSeq protein database (NCBI), using Mascot version 2.4.01 (Matrix Science, London, UK). Western botting analysis was used to detect the retrieved protein.

RIP assays

In this study, the Magna RIP RNA-binding protein immunoprecipitation kit (Millipore, MA, USA) was utilized to conduct RIP assays. In brief, cells that grow in 10-cm dishes were lysed in lysis buffer (0.5 mL) containing protease inhibitors and RNase inhibitor (Thermo Fisher Scientific, Rockford, IL, USA) and centrifuged at 12,000 rpm for 30 min. The supernatants were incubated with Protein G Dynabeads (Thermo Fisher Scientific, Carlsbad, CA, USA), which were incubated with the indicated antibodies for 12 h at 4°C with rotation. The beads were washed three times with wash buffer containing RNase inhibitor and then twice with PBS containing RNase inhibitor. The RNA was extracted by using the total RNA isolation kit (Thermo Fisher Scientific), and quantitative real-time PCR was performed as described above.

In vivo assays

Female athymic BALB/c nude mice (4–5 weeks old) were purchased from the Experimental Animal Center of Shanghai Cancer Institute (Shanghai, China). Mice (five in each group) were injected subcutaneously with 0.2 mL of cell suspension containing 5×10^5 cells (siNC and siRP11-616M22.7 stable GIST-T1 cell line) in the right axilla. The treatment groups were treated with imatinib from day 7. When a tumor was palpable, it was measured every 3 days, and its volume was calculated according to the formula volume = (length × width^2) × 0.5 as described in the previous study.[6] Sample size was not predetermined for these experiments. All experiments were performed in accordance with relevant institutional and national guidelines and regulations of the Shanghai Medical Experimental Animal Care Commission.

Statistical analysis and plots

Data are shown as mean ± SEM (standard error of the mean) or median with the interquartile range. The differences between two groups were estimated by Student's t test or s Wilcoxon rank-sum test. The volcano and bubble plots were created by using the geom_point in the ggplot2 R package. Additionally, heatmaps were generated from the ComplexHeatmap R package.[30] All statistical computation and plots in this study were performed in the R environment.[31] Unless indicated otherwise, we considered a statistical test with a p value <0.05 significant.

SUPPLEMENTAL INFORMATION

Supplemental information can be found online at https://doi.org/10.1016/j.omtn.2021.05.017.

ACKNOWLEDGMENTS

This study was supported by grants from the National Natural Science Foundation of China (No. 81702307), the Fujian Provincial Health Career Training Project for Young and Middle-Aged Key Talents (Type B) funded by the Fujian Provincial Health Commission (2019-ZQNB-38), and the Xiamen medical and health guidance project supported by Xiamen Science and Technology Bureau (3502Z20199182 & 3502Z20209041).

AUTHOR CONTRIBUTIONS

Y.S., Y.Z., and J.W. conceived and designed the study. S.L. and J.Z. collected clinical samples and performed validation experiments in clinical samples. Y.S. performed data analysis and visualization. Y.S., S.L., H.T., J.W., and J.X. performed *in vitro* experiments. S.L., W.L., and G.H. performed *in vivo* experiments. Y.S. and Y.Z. wrote the manuscript. All authors reviewed the manuscript and gave consent for publication.

DECLARATION OF INTERESTS

The authors declare no competing interests.

REFERENCES

1. von Mehren, M., and Joensuu, H. (2018). Gastrointestinal stromal tumors. J. Clin. Oncol. *36*, 136–143.

2. Joensuu, H., Vehtari, A., Riihimäki, J., Nishida, T., Steigen, S.E., Brabec, P., Plank, L., Nilsson, B., Cirilli, C., Braconi, C., et al. (2012). Risk of recurrence of gastrointestinal stromal tumour after surgery: An analysis of pooled population-based cohorts. Lancet Oncol. *13*, 265–274.

3. Marchese, F.P., Raimondi, I., and Huarte, M. (2017). The multidimensional mechanisms of long noncoding RNA function. Genome Biol. *18*, 206.

4. Wang, K.C., and Chang, H.Y. (2011). Molecular mechanisms of long noncoding RNAs. Mol. Cell *43*, 904–914.

5. Zhang, J., Li, Z., Liu, L., Wang, Q., Li, S., Chen, D., Hu, Z., Yu, T., Ding, J., Li, J., et al. (2018). Long noncoding RNA TSLNC8 is a tumor suppressor that inactivates the interleukin-6/STAT3 signaling pathway. Hepatology *67*, 171–187.

6. Li, Z., Zhang, J., Liu, X., Li, S., Wang, Q., Di Chen, Hu, Z., Yu, T., Ding, J., Li, J., et al. (2018). The LINC01138 drives malignancies via activating arginine methyltransferase 5 in hepatocellular carcinoma. Nat. Commun. *9*, 1572.

7. Anastasiadou, E., Jacob, L.S., and Slack, F.J. (2018). Non-coding RNA networks in cancer. Nat. Rev. Cancer *18*, 5–18.

8. Yu, T., Zhao, Y., Hu, Z., Li, J., Chu, D., Zhang, J., Li, Z., Chen, B., Zhang, X., Pan, H., et al. (2017). MetaLnc9 facilitates lung cancer metastasis via a PGK1-activated AKT/mTOR pathway. Cancer Res. *77*, 5782–5794.

9. Pichler, M., Rodriguez-Aguayo, C., Nam, S.Y., Dragomir, M.P., Bayraktar, R., Anfossi, S., Knutsen, E., Ivan, C., Fuentes-Mattei, E., Lee, S.K., et al. (2020). Therapeutic potential of FLANC, a novel primate-specific long non-coding RNA in colorectal cancer. Gut *69*, 1818–1831.

10. Tan, D.S.W., Chong, F.T., Leong, H.S., Toh, S.Y., Lau, D.P., Kwang, X.L., Zhang, X., Sundaram, G.M., Tan, G.S., Chang, M.M., et al. (2017). Long noncoding RNA EGFR-AS1 mediates epidermal growth factor receptor addiction and modulates treatment response in squamous cell carcinoma. Nat. Med. *23*, 1167–1175.

11. Shen, S., Wang, J., Zheng, B., Tao, Y., Li, M., Wang, Y., Ni, X., Suo, T., Liu, H., Liu, H., and Zhang, J. (2020). LINC01714 enhances gemcitabine sensitivity by modulating FOXO3 phosphorylation in cholangiocarcinoma. Mol. Ther. Nucleic Acids *19*, 446–457.

12. Jiang, C., Li, Y., Zhao, Z., Lu, J., Chen, H., Ding, N., Wang, G., Xu, J., and Li, X. (2016). Identifying and functionally characterizing tissue-specific and ubiquitously expressed human lncRNAs. Oncotarget *7*, 7120–7133.

13. Yan, X., Hu, Z., Feng, Y., Hu, X., Yuan, J., Zhao, S.D., Zhang, Y., Yang, L., Shan, W., He, Q., et al. (2015). Comprehensive genomic characterization of long non-coding RNAs across human cancers. Cancer Cell *28*, 529–540.

14. Colak, S., and Ten Dijke, P. (2017). Targeting TGF-β signaling in cancer. Trends Cancer *3*, 56–71.

15. Derrien, T., Johnson, R., Bussotti, G., Tanzer, A., Djebali, S., Tilgner, H., Guernec, G., Martin, D., Merkel, A., Knowles, D.G., et al. (2012). The GENCODE v7 catalog of human long noncoding RNAs: Analysis of their gene structure, evolution, and expression. Genome Res. *22*, 1775–1789.

16. Sever, R., and Brugge, J.S. (2015). Signal transduction in cancer. Cold Spring Harb. Perspect. Med. *5*, a006098.

17. Harris, S.L., and Levine, A.J. (2005). The p53 pathway: Positive and negative feedback loops. Oncogene *24*, 2899–2908.

18. Yu, Y., and Feng, X.H. (2019). TGF-β signaling in cell fate control and cancer. Curr. Opin. Cell Biol. *61*, 56–63.

19. Papaspyropoulos, A., Bradley, L., Thapa, A., Leung, C.Y., Toskas, K., Koennig, D., Pefani, D.E., Raso, C., Grou, C., Hamilton, G., et al. (2018). RASSF1A uncouples Wnt from Hippo signalling and promotes YAP mediated differentiation via p73. Nat. Commun. *9*, 424.

20. Joensuu, H., Rutkowski, P., Nishida, T., Steigen, S.E., Brabec, P., Plank, L., Nilsson, B., Braconi, C., Bordoni, A., Magnusson, M.K., et al. (2015). *KIT* and *PDGFRA* mutations and the risk of GI stromal tumor recurrence. J. Clin. Oncol. *33*, 634–642.

21. Bolger, A.M., Lohse, M., and Usadel, B. (2014). Trimmomatic: A flexible trimmer for Illumina sequence data. Bioinformatics *30*, 2114–2120.

22. Dobin, A., Davis, C.A., Schlesinger, F., Drenkow, J., Zaleski, C., Jha, S., Batut, P., Chaisson, M., and Gingeras, T.R. (2013). STAR: Ultrafast universal RNA-seq aligner. Bioinformatics *29*, 15–21.

23. Li, B., and Dewey, C.N. (2011). RSEM: Accurate transcript quantification from RNA-seq data with or without a reference genome. BMC Bioinformatics *12*, 323.

24. Harrow, J., Frankish, A., Gonzalez, J.M., Tapanari, E., Diekhans, M., Kokocinski, F., Aken, B.L., Barrell, D., Zadissa, A., Searle, S., et al. (2012). GENCODE: The reference human genome annotation for The ENCODE Project. Genome Res. *22*, 1760–1774.

25. Love, M.I., Huber, W., and Anders, S. (2014). Moderated estimation of fold change and dispersion for RNA-seq data with DESeq2. Genome Biol. *15*, 550.

26. Grossman, R.L., Heath, A.P., Ferretti, V., Varmus, H.E., Lowy, D.R., Kibbe, W.A., and Staudt, L.M. (2016). Toward a shared vision for cancer genomic data. N. Engl. J. Med. *375*, 1109–1112.

27. Liberzon, A., Birger, C., Thorvaldsdóttir, H., Ghandi, M., Mesirov, J.P., and Tamayo, P. (2015). The Molecular Signatures Database (MSigDB) hallmark gene set collection. Cell Syst. *1*, 417–425.

28. Hänzelmann, S., Castelo, R., and Guinney, J. (2013). GSVA: Gene set variation analysis for microarray and RNA-seq data. BMC Bioinformatics *14*, 7.

29. Subramanian, A., Tamayo, P., Mootha, V.K., Mukherjee, S., Ebert, B.L., Gillette, M.A., Paulovich, A., Pomeroy, S.L., Golub, T.R., Lander, E.S., and Mesirov, J.P. (2005). Gene set enrichment analysis: A knowledge-based approach for interpreting genome-wide expression profiles. Proc. Natl. Acad. Sci. USA *102*, 15545–15550.

30. Gu, Z., Eils, R., and Schlesner, M. (2016). Complex heatmaps reveal patterns and correlations in multidimensional genomic data. Bioinformatics *32*, 2847–2849.

31. R Development Core Team (2016). R: A language and environment for statistical computing (R Foundation for Statistical Computing).